Available online at www.sciencedirect.com
SCIENCE DIRECT®
Journal of Nuclear Materials 335 (2004) 487–492
journal of nuclear materials
www.elsevier.com/locate/jnucmat

The influence of proton irradiation on the corrosion of HT-9 during immersion in lead bismuth eutectic

R.S. Lillard *, M. Paciotti, V. Tcharnotskaia

Materials Corrosion and Environmental Effects Laboratory, Materials Science and Technology Division, MST-6, P.O. Box 1663, MS G755, Los Alamos National Laboratory, Los Alamos, NM 87545, USA

Received 8 June 2004; accepted 23 August 2004

Abstract

The impedance properties of the oxide on the martensitic–ferritic steel HT-9 were characterized during proton irradiation at the LANSCE WNR facility. Prior to the irradiation experiment, samples were pre-oxidized in moist air resulting in an oxide scale that was on the order of 3 μm thick. Samples were then irradiated during immersion in 473 K lead–bismuth eutectic at a proton current of approximately 63 nA. To assess corrosion rate in real-time, a sinusoidal voltage perturbation was applied across the oxide surface as a function of frequency and the corresponding current response was measured. This method yielded values of oxide impedance which were used in conjunction with Wagner's oxidation theory to calculate corrosion rate. In general, proton irradiation was associated with an increase in corrosion rate.

PACS: 81.65.Mq; 61.80.−x; 73.40.Vz; 72.20.−i

1. Introduction

The structural components proposed for liquid lead–bismuth eutectic (LBE) based reactor coolant systems include austenitic and martensitic/ferritic steels. These materials, such as HT-9 (martensitic/ferritic) and SS 316L (austenitic), suffer from degradation in the form of dissolution owing to the relative high solubilities of Fe, Ni, and Cr in Pb, as well as oxidation. Traditionally, investigators have used immersion testing to characterize oxidation rate in LBE [1–3]. In these studies, post immersion oxide thicknesses have been used to calculated oxidation rate. While immersion studies may provide useful information on oxide scale formation, corrosion rates calculated from immersion experiments may be misleading for any number of reasons including non-linear oxidation rates (the Parabolic Rate Law) and metal dissolution at the oxide/LBE interface that is lattice conservative, i.e. no oxide thinning is apparent.

In a previous study we have examined the oxidation of martensitic/ferritic and austenitic steels in static LBE [4]. In that investigation samples were pre-oxidized in an air/H_2O vapor mixture prior to immersion. Pre-oxidation has been suggested as a means to passivate the steel surface prior to LBE exposure. This pre-passivation did not result in microstructural or hardness changes as previously reported [4]. Immersion of pre-oxidized HT-9 samples in LBE for 24 h resulted in the growth of an

* Corresponding author. Tel.: +1 505 667 6325; fax: +1 505 667 2264.
E-mail address: lillard@lanl.gov (R.S. Lillard).

0022-3115/$ - see front matter © 2004 Elsevier B.V. All rights reserved.
doi:10.1016/j.jnucmat.2004.08.009

additional oxide layer on top of the film formed during pre-oxidation. This oxide layer was columnar in nature. EDS maps of post immersion cross sections revealed that the inner (pre-oxidation) portion of the scale remained unchanged while the outer portion of the oxide formed during immersion in LBE grew in thickness and was Fe rich in comparison to the inner pre-oxidation scale. The observation that, during immersion in LBE a columnar Fe rich scaled formed on top of the pre-oxidation layer is evidence that the dominant growth mechanism involves Fe^{+++} cation transport from the metal/oxide interface to the oxide/LBE interface. The formation of an outer Fe rich oxide during immersion in LBE also indicates that Cr mobility in the pre-oxidation scale is considerably lower than that of Fe (kinetic demixing). Analysis of the post immersion oxide using glancing angle X-ray diffraction found that two distinct structures were present: $Fe_{x+1}Cr_{2-x}O_4$ (cubic, spinel) and $(Cr,Fe)_2O_3$ (rhombohedral, corundum). Angle resolved diffraction determined that the $Fe_{x+1}Cr_{2-x}O_4$ concentration increased with distance from the metal oxide interface while $(Cr,Fe)_2O_3$ remained fairly constant throughout. The conclusion that oxide growth occurs via cation transport from the metal/oxide interface is consistent with the O^{18} marker work on Fe–Cr high temperature scales by Barnes et al. [5] as well as the oxidation mechanism for Fe–Cr steels proposed by Benard [6,7].

In this paper we present data from real-time corrosion rate measurements during proton irradiation with a technique similar to electrochemical impedance spectroscopy. Electrochemical impedance spectroscopy has been demonstrate to produce accurate measurements of corrosion rate during proton irradiation in multiple studies [8–10]. In this paper, samples of HT-9 were pre-oxidized in moist air resulting in an oxide scale that was on the order of 3 μm in thickness. Samples were then irradiated during immersion in 473 K LBE at a proton current of approximately 63 nA. Impedance measurements were conducted with a 10 mV peak-to-peak sinusoidal voltage perturbation over the frequency range of $0.005–10^5$ Hz. Oxide impedance and capacitance were determined by measuring the real and imaginary current response to this voltage perturbation.

Impedance properties of oxide films on HT-9 during immersion in LBE have been studied previously [11]. Both oxide impedance and capacitance were measured as a function of pre-oxidation parameters as well as immersion time in LBE. For HT-9 in LBE at 473 K (oxygen saturated) oxide resistance (R_{ox}) was used to calculate ionic transport through the film (i.e. corrosion rate) using Wagner's oxidation theory. Corrosion rates for HT-9 in LBE at 473 K decreased with increasing pre-oxidation time in moist air at 1073 K. In a separate set of experiments, corrosion rate decreased as a function of immersion time in LBE for any given set of pre-oxidation parameters. It was shown for HT-9 that oxidation in LBE at 473 K (oxygen saturated) appeared to follow a linear rate law over immersion periods of approximately 200 h. Oxide thickness, calculated from impedance data, increased from approximately 10–35 μm over a 180 h immersion period consistent with post-immersion cross sections of the scale.

2. Experimental

Samples of HT-9: Fe – 12 at.% Cr, 1 Mo, 0.6 Mn, 0.5 W (martensite + 25% nom. δ-ferrite) were made by first heat treating the as received material in the following manner: samples were wrap in Nb foil, encapsulate in argon at −17.2 psig with a Ti ampoule. anneal at 1273 K for 20 h, then air cool, heated to 1373 K for 30 min. followed by an air cool to dissolve tungsten carbide particles, heated at 1131 K for 15 min. followed by an air cool to check grain size, then heated at 1053 K for 2.5 h. followed by a final air cool. Samples were then sheared from the heat treated plate stock to a final size approximately $7.6\,cm \times 0.64\,cm \times 0.080\,cm$. Samples were abraded with SiC paper to 1200 grit followed by cleaning in successive baths of acetone, ethanol, and DI water in an ultrasonic cleaner. This was followed by oxidation in moist air at 1073 K for 48 h. Following grinding, cleaning, and pre-oxidation the samples were subsequently immersed in LBE (no irradiation) for up to 72 h.

In situ LBE corrosion experiments were carried out in a furnace (Fig. 1) that was constructed from 3.8 cm o.d. 304L tubing (ultra high vacuum tubing). Heating was supplied by a 700 W band heater and regulated to within 3 K of the set point with an Omega controller and a type K thermocouple. Prior to introduction to the furnace, LBE ingots (55.5 wt% Bi, Table 1) were melted down and the slag was removed. The total volume of LBE introduced into the furnace was approximately 0.50 kg. The furnace was open to air unless otherwise indicated. As such, the LBE oxygen concentration was presumed to be saturated, approximately 1.0×10^{-6} wt% O, or 1.3×10^{-7} mole fraction [11]. Future configurations will employ a YSZ/Pt-air reference electrode to determine oxygen concentration [12,13].

Impedance measurements were conducted with a 10 mV peak-to-peak sinusoidal voltage perturbation over the frequency range of $0.005–10^5$ Hz. No applied dc potential was employed, that is, all measurements were conducted at the open circuit potential (OCP). To eliminate the effects of ground loops, a floating ground EIS system was used. In these measurements, the traditional three electrode set-up was employed. A three electrode set up was used to eliminate voltage drop associated with oxide formation on the counter electrode. In the present configuration, oxidized SS 304L

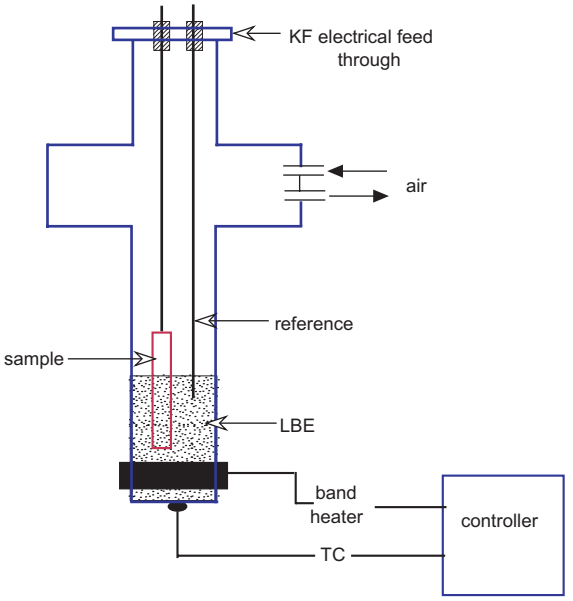

Fig. 1. A diagram of the LBE furnace used for oxide impedance measurements.

tubing (0.64 cm o.d.) was used as a reference electrode. Future configurations will take advantage of the YSZ electrode mentioned above. For constant LBE oxygen concentration as was used here, the steady state oxide formation for 304 SS in LBE reaction provides a suitably stable reference potential. Samples were welded to the end of a piece of SS 304 tubing (8.25 cm o.d., 7.9 cm i.d.) such that the sample could be suspended in the LBE furnace. At the opposite end the tubing was welded to a KF-type electrical feed-through that electrically isolated the sample from the SS furnace. The furnace wall was used as the counter electrode. To precisely center the sample in the proton beam, the furnace assembly was mount on translation stages which allowed horizontal and vertical positioning relative to the beam center line.

Experiments were conducted at the Weapons Neutron Research facility (WNR) of LANSCE. This facility provided access to the proton beam such that the furnace assembly discussed above could be used for real-time irradiation experiments and it allowed samples to be changed out routinely and safely. The flux of the incident proton beam had a Gaussian distribution of $\sigma \approx 0.7$ cm. The energy of this particle beam was 800 MeV. The pulsed beam was characterized by a gate length (macropulse) of 100 μs, a macropulse repetition rate of 100 Hz, and a fixed peak current 16 mA. These duty cycle parameters yielded an average proton beam current of 63 nA. The proton beam was centered on the sample using a phosphorous target which was lowered remotely during our EIS experiments.

3. Results and discussion

Typical Bode magnitude and phase data from HT-9 after 24 h of immersion in LBE are presented in Fig. 2 (not irradiated). The data are typical of an RC circuit with a high frequency time constant as anticipated for thin semiconducting oxide films as presented in Fig. 3. In this equivalent R_{ox} represents the oxide impedance, C_{ox} the oxide capacitance, and R_{LBE} is the geometric resistance associated with the volume of LBE and furnace configuration. Although the data may appear incomplete, C_{ox} and R_{ox} are readily obtainable from these data using a complex non-linear least squares fitting routine (CNLS). The corresponding fit of the electrical equivalent circuit in Fig. 3 to the data is also presented in Fig. 2.

The influence of proton irradiation on HT-9 oxide impedance is shown in Fig. 4(a). Prior to irradiation, oxide impedance was monitored for approximately 230 min. During this period a logarithmic increase in impedance was observed with immersion time. After 220 min the impedance appeared to be reaching a plateau on the order of 1 Ωm^2. These data are consistent with previous observations where, for multiple

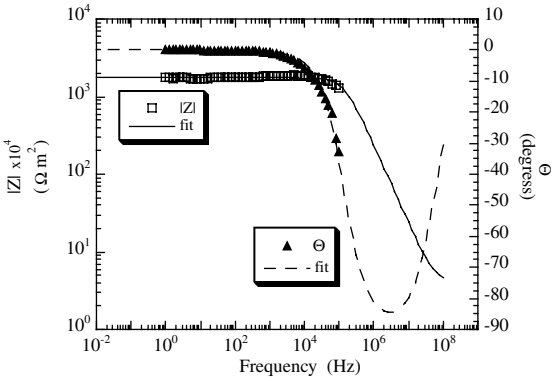

Fig. 2. Bode magnitude and phase data from a pre-oxidized (48 h at 1073 K) HT-9 sample after 24 h of immersion in LBE.

Table 1
Composition of LBE used in this investigation (wt%)

Pb	Bi	As	B	Cu	Nb	P	Sb	Sn	V	Zr
47.7	55.8	0.01	0.01	0.03	0.02	0.02	0.03	0.03	0.01	0.02

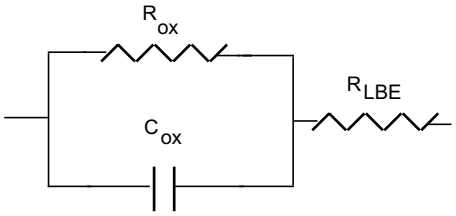

Fig. 3. Electrical equivalent circuit representing the oxide/LBE interface.

unirradiated samples, corrosion rate reached a steady state and did not diverge from that value for experiment times up to 200 h [11]. Upon turning the beam on to a value of 63 nA after approximately 240 min of immersion in LBE a sharp fall in impedance was observed. This decline in impedance continued throughout the 30 min irradiation period. After turning the beam off, oxide impedance was monitored for an additional 640 min (not all data shown). This period was characterized by widely fluctuating oxide impedance values. Similar results were observed in duplicate samples. This type of behavior was not observed in un-irradiated samples as discussed above and indicates an inability of the sample to repassivate.

Corrosion rate calculations have been preformed using experimental values of R_{ox} and Wagner's oxidation theory. This method has been discussed in detail elsewhere [11]. To summarize, the number of ions (i.e. Fe^{+++}, Cr^{+++}, ...) being transported across the scale as a function of time (dn/dt, equivalent to corrosion rate) was calculated using the relationship:

$$\frac{dn}{dt} = \frac{kT\sigma_{ox}t_i}{8be^2L}(\ln a_0 - \ln a_i), \quad (1)$$

where L is oxide thickness in m, b is the number of oxygen atoms in one M_aO_b unit, k is the Boltzman constant and is equal to 1.381×10^{-23} J/K, e is elementary charge and is equal to 1.602×10^{-19} C, a_0 and a_i are the activities of oxygen in the LBE and at the metal oxide interface (the oxide decomposition pressure at the temperature of the experiment) in mole fraction, [1] σ_{ox} is the total conductivity of the oxide in $(\Omega m)^{-1}$, and t_i and t_e is the ionic transport number. With knowledge of the transport number, oxygen activity, the corrosion rate can be calculated from Eq. (2) using the relationship for oxide conductivity:

$$\sigma_{ox} = \frac{L}{R_{ox}A}, \quad (2)$$

where A is the surface area of material exposed to LBE in m^2, L is the oxide thickness in m, and R_{ox} is the dc resistance of the oxide in Ω. Note that the substitution of Eq. (2) in to Eq. (1) results in cancellation of L, therefore, no measure of oxide thickness is required.

To calculate corrosion rate the following values were used in Eq. (1): $a_0 = 1.3 \times 10^7$ mole (from 10^7 to 10^{-7}) fraction, a_i (decomposition pressure at 473 K) ≈ 10^{-35} Pa (≈10^{-40} mole (from 10^{40} to 10^{-40}) fraction), $t_i = 0.5$, and $b = 3$. From these values and the data in Fig. 4(a) values of dn/dt (corrosion rate) were calculated. The resulting data are presented in Fig. 4(b). As seen in Fig. 4(b), transport across the scale is on the order of 10^{18} ions/m^2 s. Upon reaching the oxide/LBE interface, the ion (presumably Fe^{+++} [4]) may remain in the lattice to form new scale or be dissolved into the LBE. Here, values of dn/dt were used to calculate an approximate oxide formation rate assuming no Fe^{+++} dissolution. In this calculation it was also assumed that only Fe_2O_3 was formed [2] where $\rho = 5.24 \times 10^3$ kg/m^3 (fully dense) and an equivalent weight of 0.1597 kg/mol. It has been demonstrated for this system that immersion of HT-9 in LBE at 473 K results in the growth of an iron rich outer scale [4]. Using these values for Fe_2O_3 the resulting oxide formation rates in μm/h are presented in Fig. 4(b). While these oxide growth rates are high, they are consistent with thickness measurements from unirradiated samples immersed in LBE at the same temperature for similar times [4].

The observed increase in corrosion rate during proton irradiation may be explained by local or global changes in oxide film properties. Changes such as a pinhole that allows LBE to come in direct contact with the metal substrate are ruled out. The contact impedance for bare metal in LBE (as measured by scratching) is on the order of 0.3 Ω. This impedance acts in parallel with the oxide impedance. Thus, if a pinhole were present, one might anticipate measured impedances less than 0.3 Ω. This was not observed. Global changes such as structural, electrical, or chemical changes in the oxide seem more feasible. Electrical changes include metallization of the oxide film that may owe to Cr(III) dissolution into the melt. In addition, it is well know that proton irradiation of insulating oxides (ceramics) results in transient radiation induced conductivity (RIC) by promoting electrons from the valence band to the conduction band [14–16]. Therefore, it may be anticipated that the impedance properties of the semiconducting oxide formed on HT-9 will change during proton irradiation. Analysis of data from Mott–Schottky experiments on tungsten (W) found that the oxygen vacancy concentration in W films formed during proton irradiation were lower than those films

[1] Here we have chosen to use oxygen activity as opposed to oxygen partial pressure.

[2] We have used Fe_2O_3 as Fe^{+++} is the species transported across film. As noted in the Introduction, the outer layers formed during LBE immersion have been determine to consisted of $Fe_{x+1}Cr_{2-x}O_4$ (suggesting a mixed oxidation state). Our assumption has little impact on the conclusions in this paper.

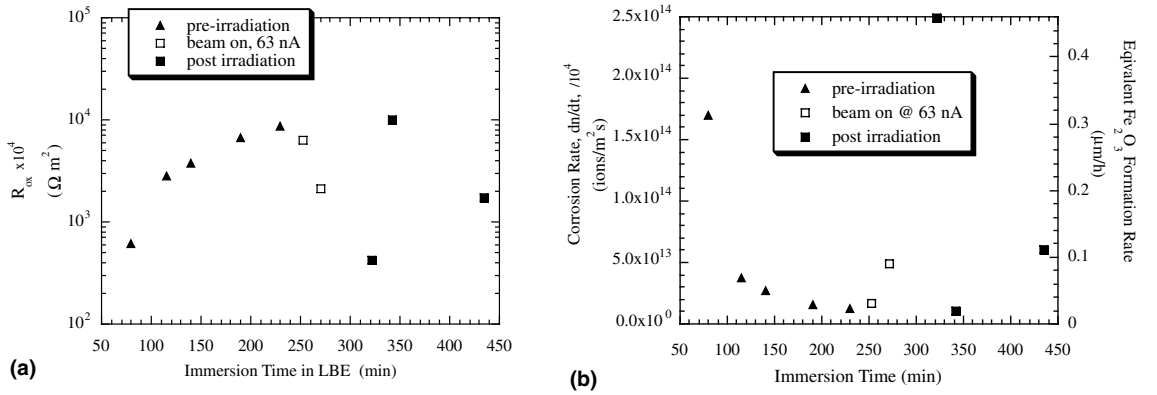

Fig. 4. (a) Oxide impedance as a function of LBE immersion time for a pre-oxidized HT-9 sample (48 h at 1073 K). Plot shows pre-irradiation, irradiation and post-irradiation data. (b) Corrosion rate data (dn/dt, calculated from Fig. 4(a) and Eqs. (1) and (2)) as a function of LBE immersion time for a pre-oxidized (48 h at 1073 K) HT-9 sample. Plot shows pre-irradiation, irradiation and post-irradiation data. Oxide formation rate assumes no Fe^{+++} dissolution and only fully Fe_2O_3 formation.

formed in the absence of irradiation [17]. The observed decrease in the oxygen vacancy concentration was also associated with higher W corrosion rates during proton irradiation. A decrease in the oxygen vacancy concentration indicates proton irradiation alters the passive film by either decreasing the oxygen vacancy flux or increasing oxygen vacancy diffusion. As it applies to the scale formed on HT-9, one might conclude that proton irradiation results in a similar change in donor concentration in the film which, ultimately, increases oxidation rate.

While the behavior observed in Fig. 4(a) was duplicated in multiple pre-oxidized HT-9 samples, it was not always observed. In a separate HT-9 experiment, a pre-oxidized sample with a higher initial impedance value maintained passivity during its initial exposure to the proton beam. The data are shown in Fig. 5. Although this sample of HT-9 was pre-oxidized in the same batch run as the sample in Fig. 4(a) (48 h at 1073 K), it had a higher initial value of oxide impedance which remained constant throughout the pre-irradiation period. Upon turning the beam on to 63 nA at approximately 160 min, no change in oxide impedance was observed. The post-irradiation period was characterized by stable, impedances that did not differ from the pre-irradiation values. While this behavior was only observed in one sample, it is possible that initial values of the oxide impedance are an indicator of irradiation properties. Further, it may be possible to optimize oxide properties to avoid the observed increases in corrosion rate during proton irradiation. As seen in Fig. 5, after removal of the sample from the LBE bath and re-immersion the oxide impedance decreased from approximately 6.0–1.8 Ωm^2. This value was closer to the steady state value of impedance observed in the sample that failed during irradiation in Fig. 4(a). Upon turning the beam on to a current of 63 nA at approximately 400 min a sharp decrease in oxide impedance was observed (Fig. 5). After

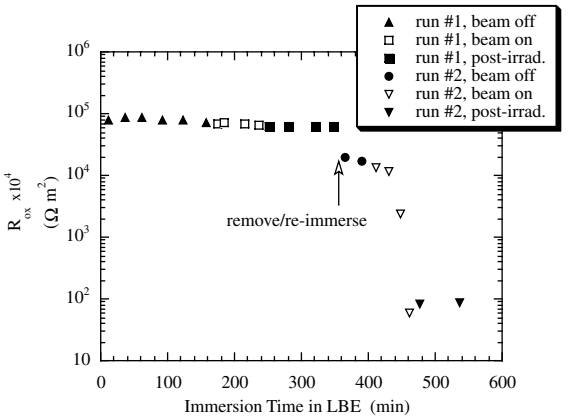

Fig. 5. Oxide impedance at 1.0 kHz as a function of immersion time in LBE. After approximately 360 min of immersion the sample was removed from the LBE furnace for several hours. The sample was then re-introduced into the furnace and measurements were continued.

turning the beam off, the impedance values remained low indicating that the irradiation induced changes in dielectric properties were irreversible. Similar observations were made for the sample tested in Fig. 4(a).

Finally, while there is a wealth of corrosion rate data from coupon studies (unirradiated) for steels in LBE, both flow loop and static immersion data, it is not clear how to relate corrosion rates from immersion data with from impedance methods. The problem arises from the method used to determining corrosion rate from a coupon. Coupon studies rely on weight change or oxide thickness changes over an immersion period that may last 100s to 1000s of hours. Therefore, the rates reflect the average behavior over the entire immersion period. Further, the oxide thickness calculations assume no

dissolution and weight change calculations assume no gain from melt (i.e. LBE migration along grain boundaries. Thus an instantaneous corrosion rate, as measured with an impedance technique is always preferable. However, we have demonstrated in previous work for short immersion times (24 h) that corrosion rates from impedance and coupon immersion studies are comparable [11].

4. Conclusions

The oxide dielectric properties of the martensitic–ferritic steel HT-9 were characterized during proton irradiation at the LANSCE WNR facility. Samples were pre-oxidized in moist air at 1073 K prior to the irradiation. To characterize the real-time oxide dielectric properties a sinusoidal voltage perturbation was applied across the sample surface and the corresponding current response from the sample was measured. In general, proton irradiation was associated with a increase in corrosion rate. The observed increase in corrosion during irradiation was attributed to global changes in chemical, structural, or electronic properties of the oxide. Unfortunately, beam-time restraints did not permit further investigation of this phenomena. However, similar increases in corrosion rate during proton irradiation of tungsten have been shown to be related to changes in the donor concentration of the within surface oxide. As it applies to the scale formed on HT-9, one might conclude that proton irradiation results in a similar change in donor concentration in the film which, ultimately, increases oxidation rate.

Acknowledgments

Work on this project was performed by the University of California under the auspices of the United States Department of Energy – NNSA, contract W7405-ENG36. The authors are grateful for the support of Mike Cappiello, Ning Li, and Kemal Pasamehmetoglu through the US DOE Advanced Fuel Cycle Initiative.

References

[1] H. Glasbrenner, J. Konys, G. Mueller, A. Rusanov, J. Nucl. Mater. 296 (2001) 237.
[2] F. Barbier, A. Rusanov, J. Nucl. Mater. 296 (2001) 231.
[3] C. Fazio, G. Benamati, C. Martin, G. Palombarini, J. Nucl. Mater. 296 (2001) 243.
[4] R.S. Lillard, C. Valot, M.A. Hill, D. Dickerson, R.J. Hanrahan, Corrosion 60 (11) (2004).
[5] D.G. Barnes, J.M. Calvert, K.A. Hay, D.G. Lees, Philos. Mag. 28 (1973) 1303.
[6] J. Benard, J. Hertz, Y. Jeannin, J. Moreau, Comp. Rend. Acad. Sci. (Paris) 248 (1959) 2095.
[7] J. Benard, Oxydation des Metaux, Gauthier-Villars, Paris, 1964.
[8] R.S. Lillard, G.J. Willcutt, D.L. Pile, D.P. Butt, J. Nucl. Mater. 277 (2000) 250.
[9] R.S. Lillard, M.A. Paciotti, J. Nucl. Mater. 303 (2001) 105.
[10] R.S. Lillard et al., in: S.T. Rosinski, M.L. Grossbeck, T.R. Allen, A.S. Kumar (Eds), Effects of Radiation on Materials, 20th International Symposium, ASTM STP 1405, Conshonhocken, PA, 2001, p. 631.
[11] R.S. Lillard, C. Valot, R.J. Hanrahan, Corrosion 60 (12) (2004).
[12] R. Szwarc, K.E. Oberg, R.A. Rapp, High Temperature Sci. 4 (1972) 347.
[13] J. Konys, H. Muscher, Z. Vob, O. Wedemeyer, J. Nucl. Mater. 296 (2001) 289.
[14] L.W. Hobbs, F.W. Clinard, S.J. Kinkle, R.C. Ewing, J. Nucl. Mater. 216 (1994) 291.
[15] G.P. Pells, J. Nucl. Mater. 184 (1991) 177.
[16] G.P. Pells, J. Nucl. Mater. 184 (1991) 183.
[17] R.S. Lillard, G.S. Kanner, L.L. Daemen, Electrochim. Acta 47 (2002) 2473.